International Nano Letters (2018) 8:165–179
https://doi.org/10.1007/s40089-018-0242-6

ORIGINAL ARTICLE

Controlled synthesis of ZnO nanoparticles and evaluation of their toxicity in *Mus musculus* mice

Julián Medina[1] · Harold Bolaños[2] · Lyda Patricia Mosquera-Sanchez[3] · J. E. Rodriguez-Paez[1]

Received: 26 December 2017 / Accepted: 22 July 2018 / Published online: 28 July 2018

Abstract

Zinc oxide nanoparticles (ZnO-NPs) of different sizes and morphology were synthesized. The variables analyzed were zinc precursor concentration, the nature of the synthesis solvent and the concentration of surfactant agent. The solids synthesized were characterized using IR spectroscopy, X-ray diffraction (XRD) and transmission electron microscopy (TEM). Considering the nature of the synthesis process, a tentative model of the mechanism of formation of the ZnO-NPs was proposed. ZnO-NPs with spheroidal morphology were obtained with a 10 mM CTAB concentration and these were selected to study their toxicity. For this study, *Mus musculus* mice were therefore given an oral dose of 50 mg ZnO/kg body weight (b.v.). Biopsies obtained from the livers and kidneys of the mice studied were analyzed using TEM and atomic absorption. The biopsy of the liver of the mouse given a dose of ZnO-NPs showed evidence of steatosis. The atomic absorption results showed the accumulation of Zn in both the liver and the kidney of the mouse.

Keywords ZnO nanoparticles · Synthesis · Characterization · Formation mechanism · Toxicity

Introduction

Zinc oxide (ZnO) is one of the most interesting inorganic compounds in the fields of science and technology [1–4]. Interest continues to grow due to the exploration of new technologies, in which the range of capabilities of ZnO already plays or may go on to play an exciting role [5] given its optical properties [6–9], its nature as a semiconductor [9–11] and the physicochemical properties of its surface [12]. The ongoing interest in this oxide rests, too, on the development of new technologies for obtaining single crystals and epitaxial layers of high quality, which constitute the basis for manufacturing electronic and optoelectronic devices using ZnO [7–11]. The ability to obtain nanoparticles and nanostructures in general has also meant an increased interest in ZnO, taking into account its potential use in fields such as environmental remediation [13–15].

ZnO crystallizes, at ambient temperature and pressure, into a wurtzite-type (type B4) structure (P63mc spatial group) [7–9]. Through theoretical calculations, it has been determined that the value of the band gap is 3.77 eV that correlates reasonably with the experimental value obtained of 3.4 eV [16]. Due to the wide band gap of ZnO and its large exciton binding energy of 60 meV at room temperature, this oxide is very attractive for applications such as optoelectronic devices.

Although ZnO is usually listed as a non-toxic material [17] and is therefore used in a wide range of cosmetic products, including moisturizers, lip products, mineral makeup foundations, face powders, ointments, lotions and hand creams [18], recent research has studied the biokinetics of ZnO-NPs, looking at toxicokinetics, biological fates and protein interaction [19, 20]. These works yielded important information about the way in which nanoparticles enter circulation systems, the target organs of accumulation and

✉ J. E. Rodriguez-Paez
jnpaez@unicauca.edu.co

Julián Medina
Julianmedina15@gmail.com

Harold Bolaños
harolbolanos@gmail.com

Lyda Patricia Mosquera-Sanchez
pmos22@gmail.com

[1] Cauca University, Zona Tulcán/Faculty of Engineering, Popayan, Colombia

[2] Faculty of Health Sciences, Cauca University, Calle 5 N° 4-70, Popayan, Colombia

[3] National University of Colombia, Palmira Headquarters, Palmira, Valle del Cauca, Colombia

toxicity, and their elimination time, important for predicting the long-term toxic potential of nanoparticles.

As is well known, the biokinetic behavior of the ZnO-NPs depends both on their physicochemical properties, determined principally by the method of obtaining them, their dissolution properties in biological fluids and the nanoparticle–protein interaction. Specifically, the toxicity mechanism of nanoparticles must depend on the physicochemical properties such as particle size, the kinetics of dissolution and retained surface species, but the understanding of the contribution of each of them to toxicity is incomplete [21, 22]. This is why studies such as that of Aula et al. [23], in which the biological interaction of ZnO-NPs with different characteristics was studied, allow us to understand the biological interaction of nanoparticles, the consequences of this interaction and the mechanism associated with the toxicity induction. ZnO powder may be dangerous if inhaled or ingested, causing a condition called zinc or zinc ague fever. The ecotoxicity of ZnO would be caused mainly by the soluble fraction of oxide, i.e., by the Zn ion [24]. The work of Eixenberger et al. [25] showed that the presence of potential buffering systems in the biological material studied dramatically impacts the dynamics of ZnO-NPs, including their kinetics of dissolution, complex precipitate formation and toxicity profiles.

ZnO has been synthesized by different methods [26–38]. To control the size and morphology of the ZnO particles synthesized, researchers have used surfactants [39], a strategy employed in the current work. A fuller study was performed by Salem and Hammad [40] to know the effect of the nature of the surfactant on the size and morphology of ZnO particles. They used three surfactants: Triton (TX-100), sodium dodecylsulfate (SDS) and cetyltrimethylammonium bromide (CTAB), and obtained wurtzite ZnO nanoparticles nearly spherical so that the nanoparticles produced using CTAB presented the smallest size. As shown by the results of work with other systems [41], the behavior and functionality of the particle, together with its toxicity, can significantly affect the method of synthesis and processing history. To understand and predict the behavior of nanoparticles, it is therefore necessary to ensure the reliability and reproducibility of the method of production. Although many stages of the synthesis process are well understood and reproducible in the hands of expert researchers, the results of Karakoti et al. indicated that small and apparently insignificant differences can strongly alter the properties of the final product [41]. Kumar et al. [42], for example, showed that small modifications in the synthesis process could strongly impact the biological and toxicological activity of ceria, and its functionality in general, so that the reproducibility of the synthesis of materials is often a challenge.

On the other hand, given the potential applications of these nanoparticles, for example in therapeutics or drug delivery applications, it is important to develop an in-depth understanding of the biological interaction of NPs at the points of contact in the body and to determine the potentially dangerous biological effects. This field of knowledge has generated great interest, which has led to give a special name: “nanotoxicology” [43, 44]. The main objective of nanotoxicology is to study the interactions of nanoparticles with organic molecules such as proteins, lipids or nucleic acids, actions that can modify the retention and properties of nanoparticles in the body. A study to evaluate the acute toxicity of oral exposure of nano- and microscale zinc powder in healthy adult mice was conducted by Wang et al. [45]. The mice were administered gastrointestinally, at a dose of 5 g/kg body weight, two particle sizes: nanoscale zinc (N-Zn) and microscale zinc (M-Zn) powder. Mice treated with N-Zn had more severe symptoms of lethargy, vomiting and diarrhea in the beginning of the treatment than the M-Zn mice. The work of Sharma et al. [46] demonstrated that on administering sub-acute oral doses of ZnO-NPs to mice, there was a resulting accumulation of nanoparticles in the liver, causing oxidative stress, mediated DNA damage and apoptosis. The study of Zhang et al. [47] showed that depending on the concentrations used, the effect of the ZnO nanoparticles varied. These researchers concluded that the difference in toxicity for different ZnO particles depends mainly on the effect of nondissolved ZnO particles. Meanwhile, Pasupuleti et al. [48] determined the significance of dose by comparing the acute oral toxicological potential of nano-sized and micro-sized zinc oxide. The effect of ZnO micro- and nanoparticles on biochemical and hematological parameters was analyzed, finding that microscopic lesions in the liver, pancreas, heart and stomach of Sprague–Dawley rats were higher for small doses of nano-size zinc oxide than for higher doses.

In this paper, ZnO nanoparticles were successfully synthesized. The three variables examined were zinc precursor concentration (zinc acetate dihydrate), the nature of the solvent used in the synthesis (ethanol and ethylene glycol) and the concentration of surface-active agent (CTAB). Of the synthesized nanoparticles, the one that showed the best dispersion and a size of less than 50 nm was selected to study its toxicity. Considering that in the possible therapeutic and/or diagnostic applications of ZnO-NPs, they would be administered orally or by parenteral routes, in this trial an oral dose was given to *Mus musculus* mice, containing the selected ZnO synthesized nanoparticles. Considering the recommendations of Oberdorster on the interpretation of the results of the toxicological studies using high doses [43, 44], because the NPs could agglomerate and not penetrate inside the cells, and that the greatest microscopic lesions in liver, pancreas, heart and stomach have been observed when using small doses of ZnO-NPs [48], in this work a dose of 50 mg ZnO/kg body weight (b.v.) was used. The choice of dose was made considering the influence it has on the biological

activity of NPs and the fact that it has already been used successfully by other researchers [48]. This work seeks to provide some elements of interest about aspects of the toxicity of ZnO-NPs synthesized by a chemical route in a liquid medium, from a preliminary safety standpoint.

Materials and methods

Obtaining ZnO nanoparticles (ZnO-NPs)

To synthesize zinc oxide nanoparticles (ZnO-NPs), an experimental design was carried out taking into account principally three variables: concentration of Zn precursor (dihydrated zinc acetate 99%—Merck) in solutions of 0.01–0.1 and 1 M; the nature of the solvent used in the synthesis (99.97% absolute ethanol—Merck, and ethylene glycol—Fisher); and the concentration of the surfactant agent (cetyltrimethylammonium bromide CTAB 99.97%—Merck) in solutions of 0–10 and 50 mM. A further variable that may affect the physicochemical characteristics of the ZnO-NPs is the temperature at which they require to be treated to obtain the oxide of interest. In this work, the results of previous studies were used [27, 49], ~400 °C, a suitable temperature for removing the organic phase and not too high so as not to significantly affect the characteristics of the final product.

To solubilize the reaction reagents, calculated amounts of zinc acetate and CTAB were added to a 250 mL beaker, depending on the desired concentration of the precursor (0.01–0.1 or 1 M) and surfactant (0–10 or 50 mM) in the system, respectively; finally, the solvent to be used, ethanol or ethylene glycol, was added, bringing the solution to a constant volume of 200 mL, under continuous stirring. This mixture was subjected to moderate heating at 55 °C to accelerate the dissolution process, and when it reached a homogeneous condition the system continued to be stirred for at least an hour, allowing it to reach room temperature.

To hydrolyze the homogeneous mixture and form the particulate gel, a 25% ammonia solution was added to the above mixture, under continuous stirring, to bring it to a constant pH of 8.5. The system was allowed to stand for 1 h and, as no turbidity was observed in the solution, one milliliter of ammonia solution was added periodically until turbidity was observed. Subsequently, the colloidal suspension was stirred for 5 h, covered to prevent contamination with external impurities and aged for 24 h.

The gel formed was centrifuged at 6000 rpm to separate the solid and liquid phases of the slurry. The precipitate, resulting from centrifugation, was placed in a crucible and this was placed in an oven for drying and subsequent calcination (400 °C). For this, a heating program was carried out at a heating rate of 2 °C/min.

Characterization of synthesized ceramic powders

Having obtained the samples through the synthesis process described above, the solids were subsequently observed using transmission electron microscopy—TEM, using a JEOL JEM-1200EX, to determine both the degree of dispersion of the sample and the size and morphology of its particles. These microscopy techniques made it possible to determine which ones were the samples of interest for the nanotoxicity study, i.e., those that were well dispersed and that had a nanometric size.

The selected samples underwent IR spectroscopy to determine the functional groups present in the samples, using the Thermo Electron Nicolet IR200 equipment. The sample to be tested was obtained by mixing dry KBr with the synthesized solid in a concentration of approximately 10% and the sweep was conducted between 4000 and 400 cm^{-1}. To ensure the presence in the sample of ZnO as the only crystalline phase, X-ray diffraction was used, employing a Rigaku RINT2000 (42 kV/120 mA) diffractometer, with CuK radiation, using K_a of the Cu ($k = 1.542$ Å) and the sweep was conducted between 10° and 80°.

Pre-mortem biological experimentation on *Mus musculus*

With the ZnO nanoparticles well dispersed, their toxicity was then determined, taking as reference the toxicity of commercial ZnO microparticles (99%—Merck). To carry out this experimental part, the protocol suggested by the OECD for testing fixed dose acute oral toxicity [50] was used. The mice (*Mus musculus*) used were donated by the animal facility of the University of Cauca and their age was 10 and 11 weeks. All tests were performed in a location provided for that purpose within the university, taking into account that described in the OECD-420 protocol [51].

Initially, a preliminary test was conducted to determine the dose to be used in the main study. To carry out the latter, three experimentation groups each with three mice were considered: a control group and two study groups that were given the same dose of ZnO using suspensions of micro (commercial) and nanoparticles (synthesized), looking out for the welfare of the animals. In the end, a dose of 50 mg ZnO/kg body weight (b.v.) was chosen, taking into account the suggestions of Oberdorster on the interpretation of results of toxicological studies using high doses [43, 44], the influence of the dose on the biological activity of NPs and because this dose has already been used successfully by other researchers [48]. Therefore, the diet supplied to the mice comprised a food commonly used to feed animals (Purina brand), in pellet form, and the doses of both micro and nanoparticles in a concentration determined by a preliminary study [50 mg ZnO/kg body weight (b.v.)]; these

doses were administered by means of suspensions in drinking water, every other day during a 14 day period. After carrying out this part of the test, the animals were killed by dislocation of the spinal cord.

Having carried out the euthanasia of the mice, the liver and both kidneys were removed, which were labeled and immediately frozen. A sample of about 50 mg was taken of both liver and kidney to obtain the biopsies required for TEM analysis. The rest of the excised organs were used for quantifying the Zn present in the samples, using atomic absorption spectroscopy (GBC Avanta E model).

Obtaining biopsies for TEM analysis

50 mg of both liver and kidney obtained from the killed mice was placed in a glutaraldehyde solution (25% Merck) for preservation. The process for fixing the sample in the resin was carried out following the protocol normally used for the purpose [52]. After having the sample fixed to the resin, it was sliced into 60 nm-thick sections with the help of an ultra-microtome LEICA UCT, 706201. The sections were collected in wire mesh and contrasted using uranyl citrate (25%—Fisher) and lead acetate (25%—Fisher). These sections were placed on copper grids coated with Formvar film.

Quantification of Zn present in the biological samples using atomic absorption spectroscopy (AAS)

The analysis was performed according to the provisions in Ref. [53], the only difference being that the samples were determined at 50 mL rather than at 25 mL, as indicated, and no dilution of any kind was performed on the samples before measurement; calibration of the atomic absorption spectroscopy equipment (GBC Avanta E model) was carried out between 0.1 and 1.6 mg/L.

Results and discussion

Synthesis and characterization of ZnO nanoparticles

Considering the variables of interest, 18 synthesized samples were obtained in total, labeled as indicated in Table 1.

Following the calcination process at 400 °C, to which all of the samples were subjected during their synthesis, different shades were found, ranging from white to black, with yellow being the predominant color. This difference in the color of the ceramic powders synthesized can be explained considering changes in the stoichiometry of the oxide, $Zn_{1+x}O$, which would cause differences in the structure of defects present in the solids [54] or, in the case of black color, the presence of some carbonated phase (an oxycarbonate of zinc, for example) due to the reaction on the surface of the nanoparticles of Zn^{2+}, oxygen and carbon (from the organic compounds used during the synthesis process), a reaction that would be favored as the concentration of the organic compounds in the system increased during synthesis: samples M13 to M18 and which were synthesized using 50 mM surfactant (Table 1). Alternatively, the black color in some of the zinc oxide samples may be explained as the spontaneous growth of $ZnCO_3$ on "unstable" nanostructures of ZnO, as reported by Pan et al. [55].

Table 1 Identification of synthesized samples and synthesis conditions employed (all were treated at 400 °C/2 h at the end of the process)

Sample	Zinc acetate (M)	Synthesis solvent	CTAB (mM)
M_1	1	Ethanol	0
M_2	1	Ethylene glycol	0
M_3	0.1	Ethanol	0
M_4	0.1	Ethylene glycol	0
M_5	0.01	Ethanol	0
M_6	0.01	Ethylene glycol	0
M_7	1	Ethanol	10
M_8^a	1	Ethylene glycol	10
M_9	0.1	Ethanol	10
M_{10}^a	0.1	Ethylene glycol	10
M_{11}	0.01	Ethanol	10
M_{12}^a	0.01	Ethylene glycol	10
M_{13}	1	Ethanol	50
M_{14}	1	Ethylene glycol	50
M_{15}	0.1	Ethanol	50
M_{16}	0.1	Ethylene glycol	50
M_{17}	0.01	Ethanol	50
M_{18}	0.01	Ethylene glycol	50

[a]The ZnO nanoparticles in these samples were observed in greater quantities and with a good dispersion

In the synthesized samples where no surfactant was used (M1–M6, Table 1), some nanoparticles were found (see Fig. 1). The amount of these was low, however, with a greater presence of particle agglomerates that could not be removed by applying ultrasound.

An IR spectrum characteristic of the set of samples that were obtained without the addition of surfactant is illustrated in Fig. 2 (IR spectrum corresponding to sample M6); in it a broad band is observed, starting at approximately 500 cm^{-1} and ending near 400 cm^{-1}, which may be associated with the vibrational mode of tension of the Zn–O functional group of ZnO [56].

To determine the effect of the surfactant, CTAB, on the final characteristics of the ceramic powders synthesized, different concentrations of this compound were used (see Table 1). It is worth highlighting the case of the samples synthesized using a concentration of 50 mM of the surfactant,

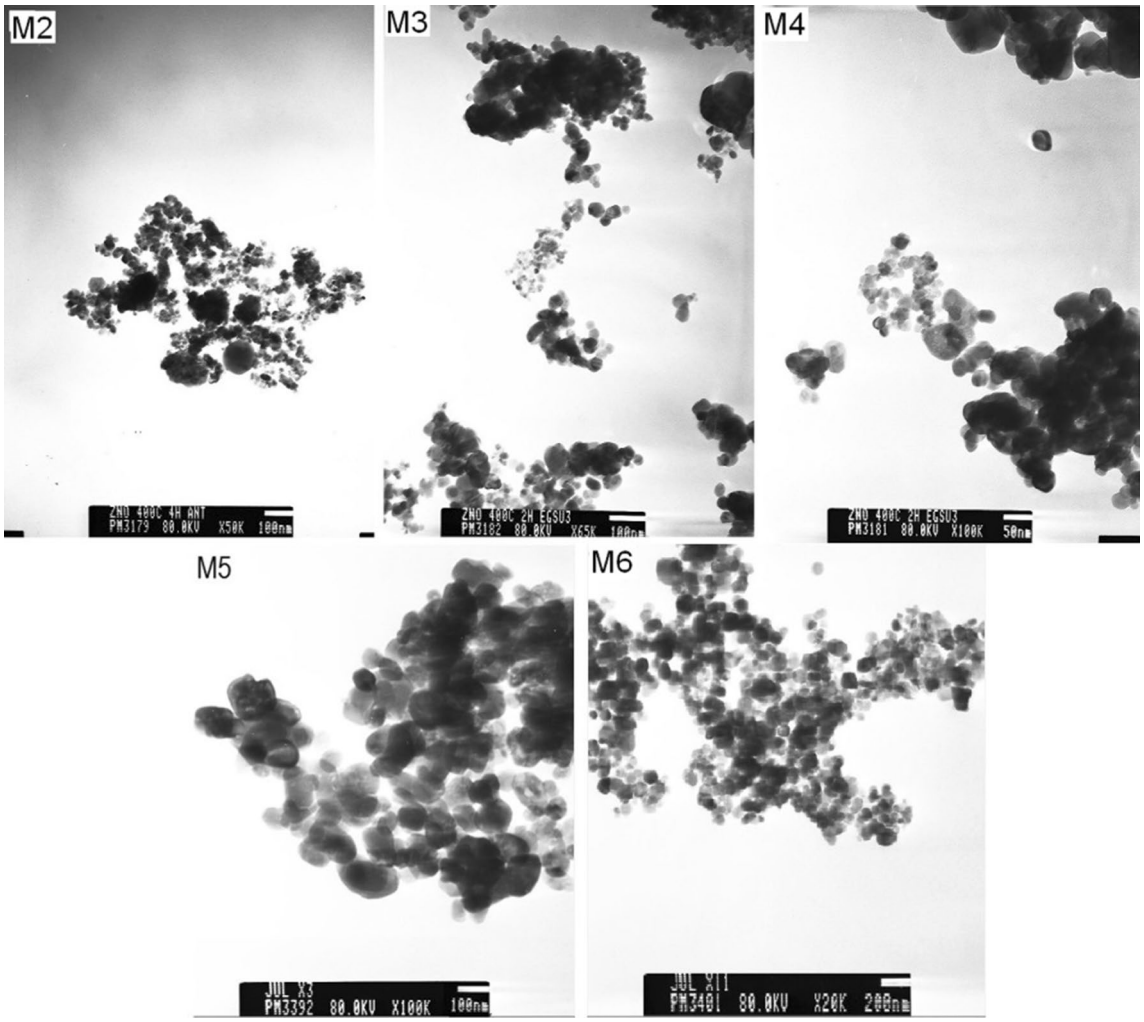

Fig. 1 TEM images of samples M2–M6 where no surfactant was used in the synthesis process

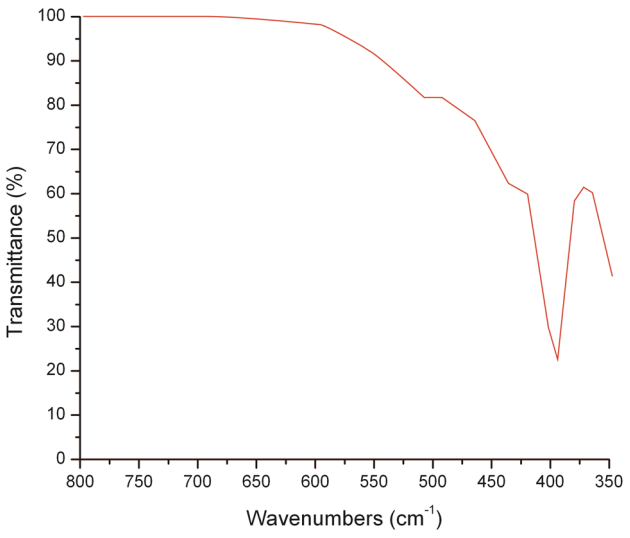

Fig. 2 IR spectrum of sample M6, obtained without the addition of surfactant. This IR spectrum is characteristic of all samples synthesized without the presence of CTAB (M1–M6 in Table 1)

which produced a black color (samples M13–M18). Figure 3 shows the images obtained with TEM of samples M13–M18, synthesized using a high surfactant content (50 mM CTAB—Table 1). The agglomeration of the particles is very evident in these samples and this prevented the approximate size of the nanoparticles being determined. Attempts were made to undo the agglomeration, subjecting the samples to the action of ultrasound for 3 h, but without success. Sample M17 was the only sample in which ZnO nanoparticles were observed (Fig. 3). The morphology of these nanoparticles was not uniform, but sheet-like or plate-like. Meanwhile, in the samples synthesized using ethylene glycol as solvent (M14, M16 and M18, Table 1), no prevalence of ZnO-NPs was observed (Fig. 3). The secondary particles (agglomerates or aggregates of nanoparticles) had sizes ranging between 200 nm and 1 μm, with an irregular morphology; samples M13 and M15 had an irregular morphology and were larger than 100 nm (submicron particles). The absence of well-dispersed ZnO nanoparticles was expected in samples M13

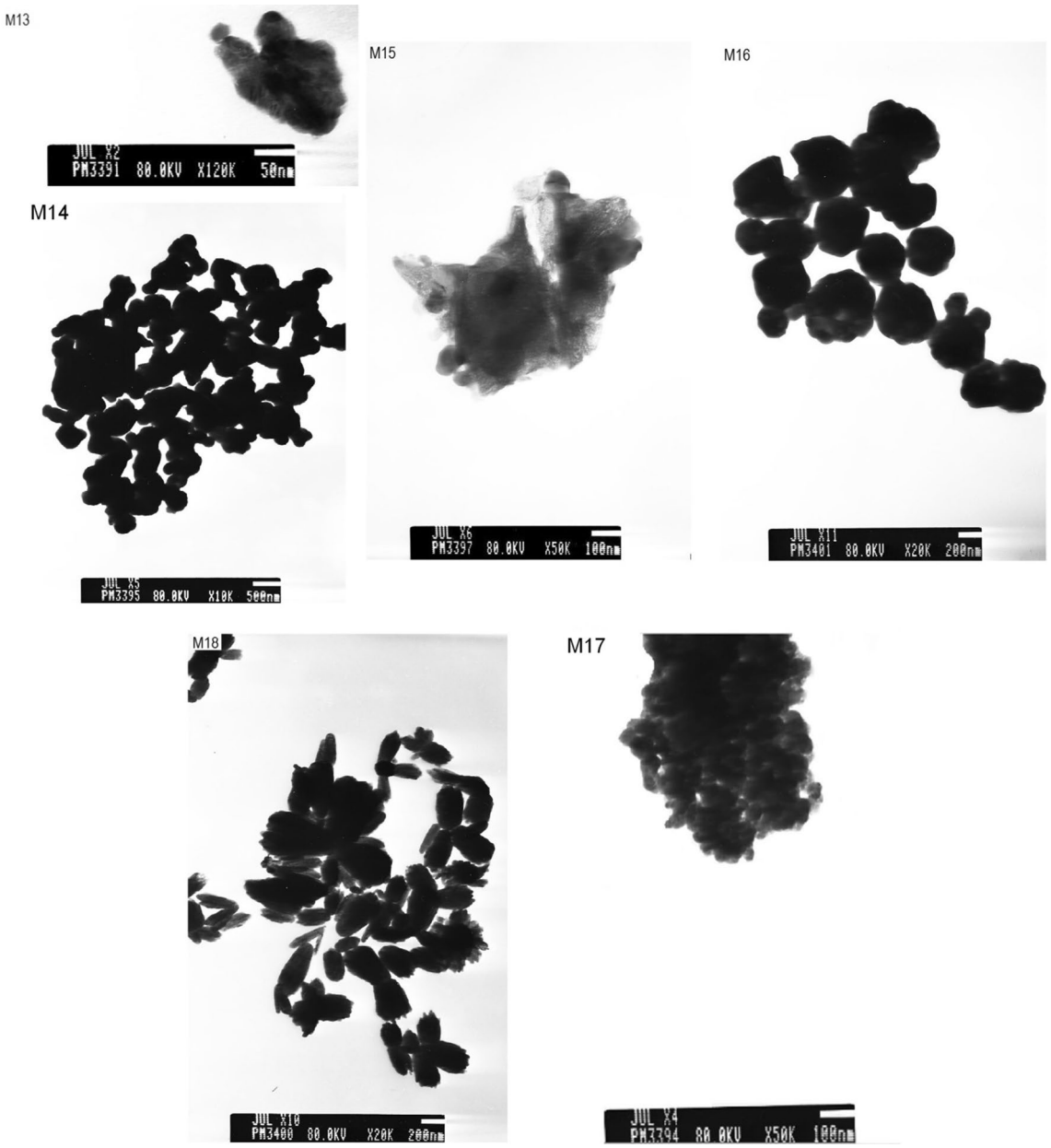

Fig. 3 TEM images of samples synthesized using solvents ethanol (M13, M15 and M17) and ethylene glycol (M14, M16 and M18), with different initial concentrations of zinc precursor: 1 M (M14 and M13), 0.1 M (M15 and M16) and 0.01 M (M17 and M18) and a high surfactant content (50 mM)

and M15, as the concentration of the zinc precursor was high (Table 1). On the other hand, low concentrations of precursor, as was the case with M17 (Table 1), would favor the formation of nanoparticles (Fig. 3), since after the formation of nuclei in the solid phase, few ions would be present in the medium, or few growth units, that would enable their growth in an appreciable way, thereby favoring the formation of ZnO-NPs [27, 49].

Meanwhile, in the photographs of samples M14, M16 and M18, Fig. 3, it can be seen that a high concentration of surfactant is not suitable for obtaining nanoparticles of ZnO and that there must be an optimum surfactant concentration that may be related to the critical micelle concentration (CMC), although for this work the aim was not to obtain mesoporous nanostructures. In the M14 sample, Fig. 3, it can be seen that for the synthesis conditions used in their production, the formation of sheet-like particles with a length ranging between 1 and 2 μm is favored, while in the M16 sample, sheet-like particles or submicron plates with dimensions ranging between 200 and 400 nm

are more evident, and in M18 the planar particles were smaller, of the order of 100 nm; this last result can be explained taking into account the low concentration of the zinc precursor, 0.01 M, used in their synthesis. It should be indicated that in the case of the samples synthesized in ethylene glycol, on evaporating the solvent by direct heating, a very viscous, transparent resin was produced, which solidified on reducing the working temperature below 100 °C, and a particulate material could not be obtained; this resin likely corresponds to an organic complex that was formed when the surfactant, CTAB, present in the system in a relatively high concentration (50 mM) reacted with the ethylene glycol. Nevertheless, the resin was burned and it was possible to obtain ZnO powders by this method. This phenomenon was not observed during the synthesis of the other samples.

The TEM images of samples M7–M12, synthesized using 10 mM of CTAB (Table 1), are shown in Fig. 4. All the samples showed ZnO nanoparticles in large quantities, with a low agglomeration. Of these, sample M8 was chosen for the nanotoxicity tests with mice, as it showed low agglomeration, good dispersion and uniform spheroidal nanoparticles with a size of ~ 50 nm.

IR spectra corresponding to samples M7–M12 (Table 1) between 800 and 400 cm^{-1} are shown in Fig. 5, in which a high intensity peak is observed at 410–450 cm^{-1} and another of lower intensity at 485 cm^{-1}, characteristic of ZnO [56].

Sample M8, chosen for the nanotoxicity studies, was characterized using XRD. Its diffractogram is shown in Fig. 6. In this, it is clear that the only crystalline phase present in the sample is ZnO (PDF 36 1451), well crystallized, with a wurtzite-type crystal structure.

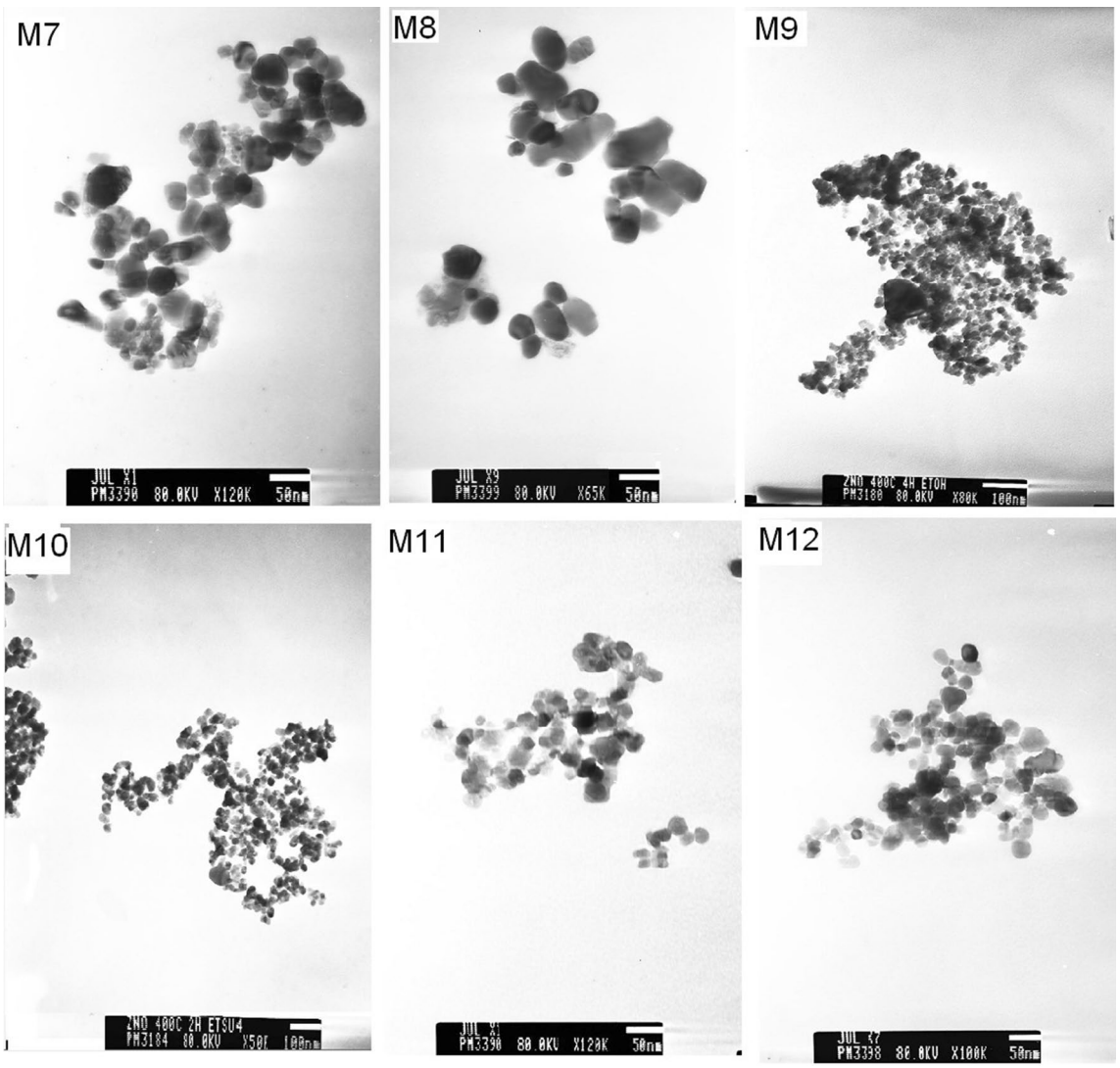

Fig. 4 TEM images of samples M7–M12 synthesized using 10 mM CTAB and solvents ethanol (M7, M9 and M11) and ethylene glycol (M8, M10 and M12)

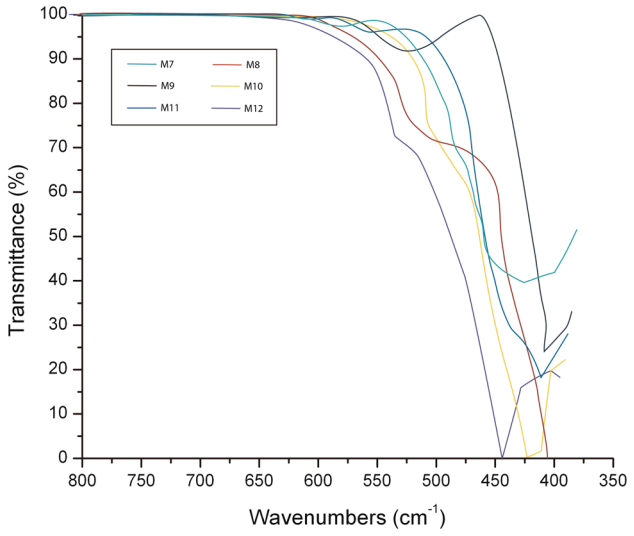

Fig. 5 IR spectra corresponding to samples M7–M12 synthesized using 10 mM CTAB and solvents ethanol (M7, M9 and M11) and ethylene glycol (M8, M10 and M12)

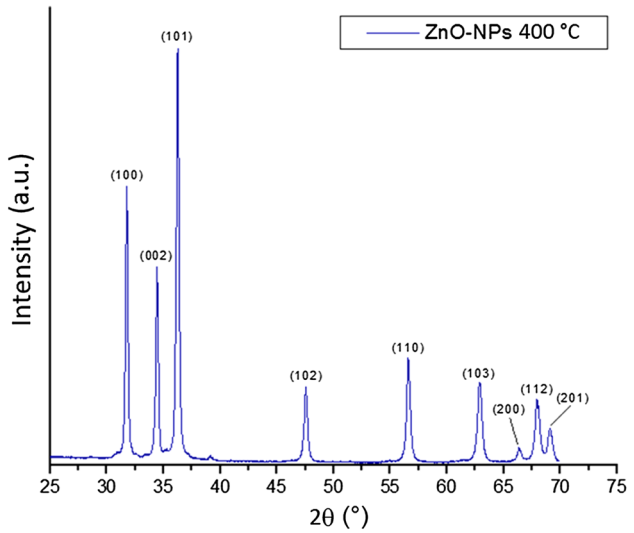

Fig. 6 X-ray diffractogram corresponding to sample M8 heat treated to 400 °C

Tentative mechanism of formation of ZnO nanoparticles

To justify the formation of the ZnO nanoparticles within the solution, account ought to be taken of the basic theory of particle growth and the chemical reactions leading to the formation of nuclei through the process of hydrolysis of Zn^{2+}. This process is favored by increasing the concentration of OH^- ions through the addition of ammonium hydroxide. The reactions that ought to predominate during the formation of the nuclei are the surface ones, due to the high ratio of surface atoms to bulk atoms in the nanoparticles. One of the first reactions that would have to take place within the solution would be the following:

$$= Zn^{2+} + OH^- \rightarrow = ZnOH^{1+}, \quad (1)$$

where $=Zn^{2+}$ represents the Zn that is linked to the nucleus of the particle in formation, located on its surface. This core would be stable and would not show phenomena of ion exchange and/or of ligands, across its surface, so that it would be the adhesion of aquo-hydroxo species of Zn, mainly $[Zn(OH)_4]^{2-}$, or zinc chemical complexes, which would facilitate the growth of the particle. Considering the Lewis acidity of Zn^{2+} ions, in solution, and the addition of ammonium hydroxide, the equilibrium represented in Eq. 2 might be favored:

$$= ZnOH + Zn^{2+} + OH^- \rightarrow = ZnOZnOH^{1+} + H^+. \quad (2)$$

The $=ZnOZnOH^{1+}$ species would continue reacting through reactions similar to that shown in Eq. 2. Taking Eq. 2 as a reference, any substance that is anionic or nucleophilic in character can generate an equilibrium of this nature, such as those illustrated in Eqs. 3, 4 and 5.

$$= ZnOH + Zn^{2+} + NH_3 \leftrightarrow = ZnOZnNH_3^+ + H^+, \quad (3)$$

$$= ZnOH + Zn^{2+} + CH_3COO^- \leftrightarrow = ZnOZnCH_3COO^- + H^+, \quad (4)$$

$$= ZnOH + Zn^{2+} + H_2O \leftrightarrow = ZnOZnOH_2^+ + H^+. \quad (5)$$

To determine which of the reactions outlined in Eqs. 2, 3, 4 and 5 is the one that controls the nucleation process of the solid phase in the system, it is necessary to consider the activities of the participating species in such equilibrium. If the medium is sufficiently basic, it is highly likely that equilibrium 2 would predominate, since of all the nucleophiles present in the reaction mixture, it is the OH^- ion that is the most nucleophilic in character given that it possesses a charge and low steric hindrance.

The equilibrium generated by the organic solvents used in this work as liquid of synthesis can be expressed as follows:

$$= ZnOH + Zn^{2+} + CH_3CH_2OH \leftrightarrow = ZnOZnOCH_2CH_3 + 2H^+, \quad (6)$$

$$= ZnOH + Zn^{2+} + CH_2OHCH_2OH \leftrightarrow = ZnOZnOCH_2OH + 2H^+. \quad (7)$$

The chemical species produced by reactions (6) and (7) would be added to those generated by reactions (2) to (5), and since in practice all solutions were at pH 8.5, equilibrium 2 would predominate in the process.

An important parameter to consider during particle growth is the concentration of Zn^{2+} present in the solution,

since it would contribute to a shift of equilibrium to the right in all of the proposed reactions. If the Zn^{2+} concentration is low, particle growth would be inhibited more quickly than for higher concentrations, an action that may be explained taking into account the following reaction:

$$= \mathrm{ZnOH} + X\mathrm{Zn}^{2+} + (X+1)\mathrm{OH}^- \leftrightarrow = \mathrm{ZnO(OZn)}x\mathrm{OH} + X\mathrm{H}^+. \quad (8)$$

The value of X would depend mainly on the concentration of Zn^{2+} in the system, so that the higher this value, the larger is the expected size of the resulting particle. Growth of the particle would also be determined by the number of nuclei formed in the solution (quantity of =ZnOH in Eq. 8), obtaining small particle size either for low concentrations of the starting zinc precursor, $Zn(CH_3COOH)_2$ (low value of X), or for a high number of nuclei formed in the solution during the process (large amount of =ZnOH in the system—Eq. 8).

Furthermore, on adding the surfactant CTAB to the system, CTA^+–$[Zn(OH)_4]^{2-}$ ion pairs should be formed that would have to affect the growth of the solid nuclei. During the reaction that occurs within the system, the CTAB would behave as template and as a means of transport for the $[Zn(OH)_4]^{2-}$ growth units [57]. These species would unite to go on to form nanospheres, for CTAB concentrations of 10 mM, independent of the nature of the solvent used in the synthesis (Fig. 4). When the dosage of CTAB was increased to 50 mM, the nanospheres tended to conglomerate to form the two-dimensional submicron plate structure to lower surface energy. These plates of ZnO were larger in size, between 100 and 400 nm (Fig. 3). Another reaction that may occur in the system would involve surfactant molecules and acetate groups, so that molecules of zinc acetate (negatively charged) would bind to the micellar head group region (where ammonium groups that are positively charged are located) due to electrostatic interaction that would be generated between them, leading to the zinc acetate precursor being localized on the micellar surface. This would cause the micellar surface to become a preferred reaction site due to the formation of highly polar intermediaries, given the high polarity of the micellar surface [40]. In summary, addition of the surfactant CTAB can affect the nucleation of the solid phase as well as growth of the particles, their coagulation and possible flocculation.

Furthermore, the presence of the CTAB molecules adsorbed on the nanoparticles would cause steric effects that would prevent their agglomeration [40, 57, 58], an action that is observed in Fig. 4. Furthermore, when samples M7, M9 and M11 are compared with samples M8, M10 and M12, Fig. 4, it can be seen that the nature of the solvent does not affect the size or morphology of the final particle. However, the initial concentration of the zinc precursor $[Zn(CH_3COOH)_2]$ is a parameter that has an important influence: the average particle size of M7 and M8 (1 M zinc acetate concentration) is approximately 50 nm, while for M11 and M12 (0.01 M concentration) it is 30 nm, reiterating the above statement that if the concentration of $[Zn(CH_3COOH)_2]$ is reduced, the formation of small particles would be favored.

In order to obtain the ZnO-NPs, both the CTAB-free and the surfactant-containing samples were thermally treated at 400 °C to remove the organic phase present therein and promote the zinc hydroxide to zinc oxide transformation (see Eqs. 2, 3, 4, 5, 6, and 7).

Toxicity testing of synthesized ZnO-NPs

Preliminary study to determine the dose of ZnO nanoparticles

For this study, ZnO-NPs from sample M8 were used (Table 1 and Figs. 1, 5, 6 and 7) together with the protocols established by the OECD [51]. These protocols indicate that for any oral toxicity study with a fixed dose, a preliminary study should be conducted to determine the most suitable dose to ensure animal welfare, avoiding swallowing effects in mice, for example. To carry out the toxicity test, a dose of 50 mg ZnO/kg body weight (b.v.) was chosen taking into account the suggestions of Oberdorster [43, 44] and because it has already been used successfully by other researchers [48]. This dose was used in this study for both nanoparticles (NPs) and microparticles (MPs) of ZnO.

Dose administration to mice

As was outlined in the experimental procedure, the dose was given to the mice every other day, as established in the protocol [51]. On the day the mice were given the dose, they were weighed and the data shown in Table 2 were obtained. From the information in the table, the decrease in weight of mice exposed to the dose can be observed (Fig. 7), greater in those where the dose was ZnO nanoparticles, as indicated by the curves in Fig. 7.

The decrease in weight shown by the mice administered with doses of ZnO containing micro or nanoparticles was the first parameter evaluated to show the negative effect of this action on the health of the mice, as established by the protocol [51] (Fig. 7). In sharp contrast to the control group, whose mice showed weight variations of less than 0.25% (some with a weight gain), the mice that were administered NPs or MPs experienced a weight decrease between 21.4–22.2 and 18.1–20.9%, respectively, slightly higher in the mice given NPs doses (Table 2).

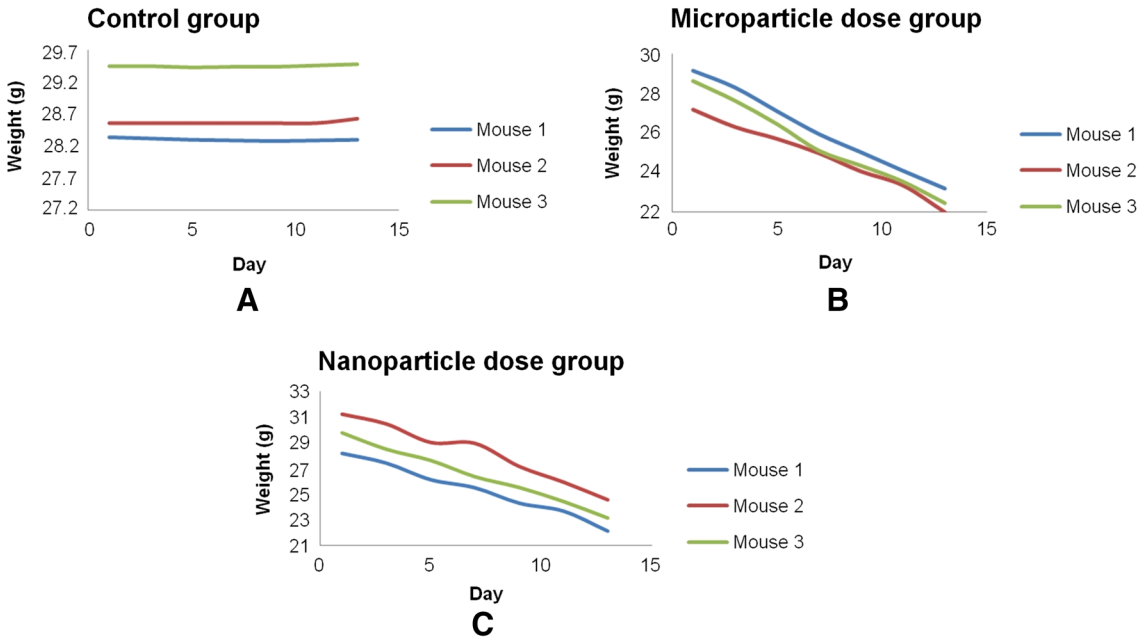

Fig. 7 Variation in weight of mice studied versus time, for control group (**a**), mice given MPs dose (**b**) and given NPs dose (**c**)

Table 2 Record of the weights of the three groups of mice studied

Group	Day 1 (g)	Day 3 (g)	Day 5 (g)	Day 7 (g)	Day 9 (g)	Day 11 (g)	Day 13 (g)	% Variation
Control, for comparison	28.34	28.32	28.30	28.29	28.28	28.29	28.30	0.141
	26.32	26.34	26.36	26.35	26.37	26.36	26.35	0.245[†]
	29.45	29.40	29.43	29.44	29.44	29.46	29.45	0.101[†]
50 mg/kg dose of microparticles	29.15	28.30	27.10	25.94	25.02	24.08	22.86	19.8
	27.18	26.30	25.70	24.97	24.05	23.34	22.80	18.1
	28.63	27.63	26.45	25.10	24.34	23.53	22.92	20.9
50 mg/kg dose of ZnO-NP	28.18	27.42	26.13	25.50	24.30	23.68	22.12	21.5
	31.23	30.47	29.03	28.96	27.16	25.94	24.56	21.4
	29.78	28.50	27.63	26.36	25.52	24.43	23.14	22.2

[†]Weight changes involved an increase, rather than a decrease

Table 3 Concentrations of Zn in liver and kidney samples of mice studied; data obtained using atomic absorption (AAS)

Group	Control (ppm)	Dose with microparticles (ppm)	Dose with nanoparticles (ppm)
Liver	11.29	18.31	20.18
	11.15	13.07	13.71
	10.77	15.84	16.17
Mean	11.07	15.74	16.68
Kidney	13.92	5.69	15.84
	8.71	19.47	16.36
	10.14	13.64	18.96
Mean	10.92	12.93	17.05

AAS analysis of bioaccumulation of Zn

To determine the accumulation of ZnO in the organs of mice administered doses of this oxide, the concentration of Zn in the liver and kidney was analyzed using atomic absorption. The results obtained are shown in Table 3.

Looking at the data shown in Table 3, the accumulation of Zn is clearly seen, relative to the control group, in both the liver and the kidney of the mice given periodic doses of ZnO particles, being greater when the dose comprised nanoparticles.

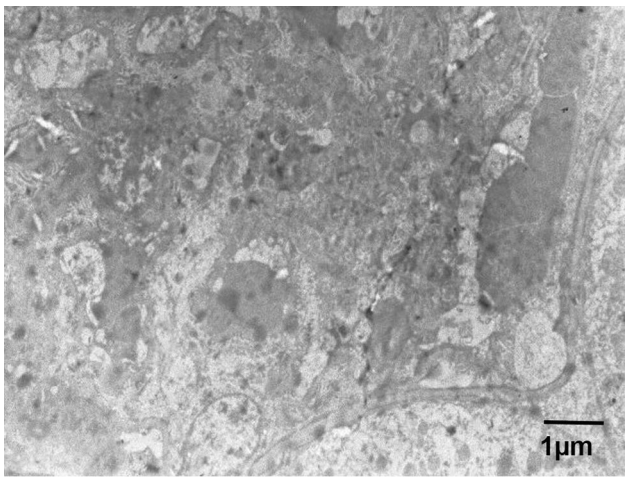

Fig. 8 TEM image of segment of glomerulus characteristic of mice group given ZnO-NP diet (magnification factor ×4000)

TEM analysis of liver and kidney biopsies

To be able to expand on the information from the AAS study, TEM analysis of liver and kidney biopsies of the specimens of interest was carried out. The analysis focused on finding pathological abnormalities in the cells of the two organs studied.

Kidney biopsies After observing and analyzing with TEM the nine kidney samples (three from each group of mice), no significant pathological changes were observed at the structural level, particularly in the nephrons (the basic units of kidney physiology). Figure 8 shows a segment of the glomerulus characteristic of the kidney of mice given a dose of ZnO-NPs. Although the data in Table 3 indicate that, for the individuals of the group given doses of NPs, a substantial bioaccumulation of Zn occurred, this condition was not reflected in the pathology (Fig. 8).

Liver biopsies The liver biopsies analyzed, obtained from the individuals from the group given a dose of microparticles, Fig. 9b, showed no significant pathological damage compared to the reference group, Fig. 9a. Although a significant accumulation of Zn occurred in the liver of the individuals given the MP dose (Table 3), this did not generate damage at the structural level in the liver cells (hepatocytes) of the mice.

In the liver biopsy of one of the individuals from the group given doses of NPs, meanwhile, a condition known as steatosis was observed. Steatosis is characterized by the accumulation of fat in the hepatocytes, as illustrated in Fig. 10. On comparing Fig. 9a with Fig. 10, the contrast between liver biopsies could be seen, highlighting the

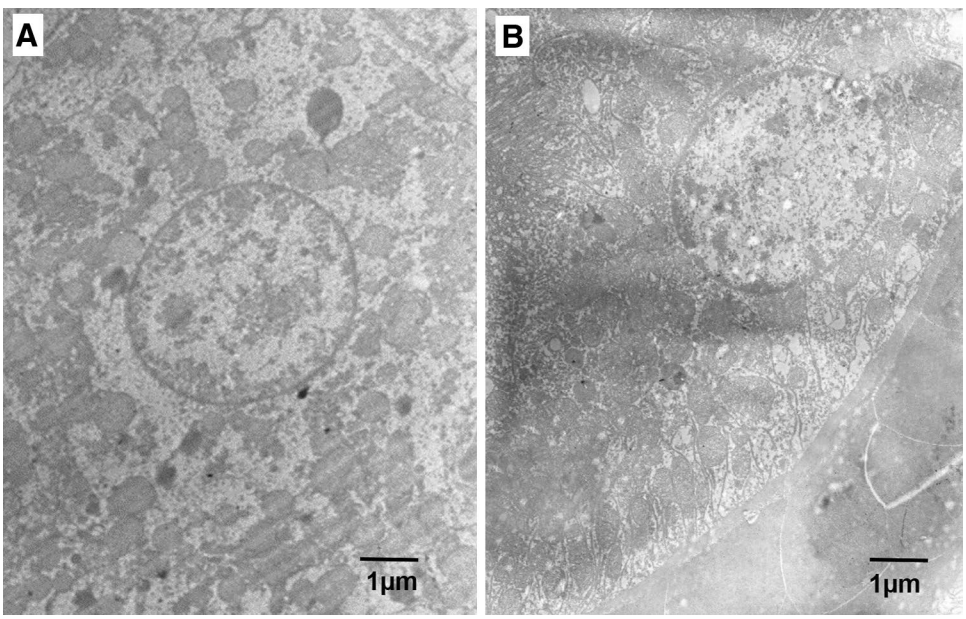

Fig. 9 TEM images of a hepatocyte corresponding to liver biopsies of individuals from the reference group (**a**) and the group of mice given doses of microparticles (**b**) (magnification factor ×4000)

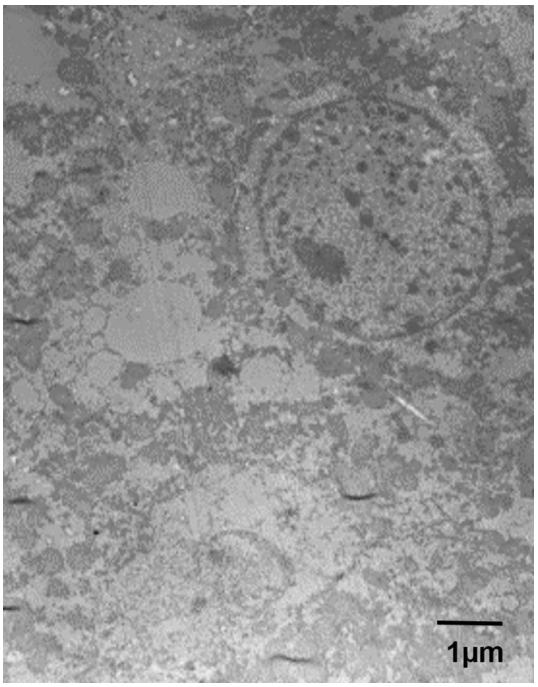

Fig. 10 TEM image of hepatocytes with steatosis (fat accumulation in liver) present in the liver biopsy extracted from a mouse from the group given doses of NP (magnification factor ×4000)

pathological effect, at the ultrastructural level, of the ZnO-NPs. In this case, the substantial bioaccumulation of Zn (Table 3) was reflected in the pathology (Fig. 10).

As indicated by Sharma et al. in their work [46], the target organ to which the ZnO-NPs were directed was the liver, being the organ most affected, even more than the kidney. They observed that after administering a dose of 300 mg/kg (for 14 days) to albino mice, the specimens showed a bioaccumulation of ZnO-NPs, mainly in the liver. A similar result was obtained in this work: a bioaccumulation of ZnO-NPs in the liver of mice but administering a dose of a lower order of magnitude (50 mg/kg) for the same 14 days. Additionally, we found that oral delivery of doses containing ZnO-NPs induced steatosis in the liver, a disease characterized by the abnormal retention of lipids within the cell. The mechanisms that cause steatosis are unclear, but it is known that this disease can be generated primarily due to a variety of alterations in the metabolic pathways of synthesis, catabolism and/or lipid transport. Lipid metabolism in the liver is an active process such that the synthesis of bile acids, synthesis of transport lipoproteins, cholesterol synthesis, catabolism of triglycerides and the formation of ketone bodies are processes that normally take place in the hepatocytes [59]. It is possible that the free radicals generated by the ZnO-NPs [60] cause lipid peroxidation and oxidative stress, inducing steatosis in the liver of the mice, specifically in specimens given ZnO-NP doses, these mice being the ones which presented this disease. In addition, ZnO-NPs could be dissociated in biological media [61] so that the release of Zn^{2+} ions can alter cellular Zn homeostasis, producing oxidative stress as well as mitochondrial and lysosomal damage [62]. Watson et al. demonstrated that dissolution of ZnO-NPs within Kupffer cells leads to extracellular release of Zn^{2+} ions and subsequent fecal clearance [62]. Alterations in the hepatic ultrastructure in rats have also been reported for nanoparticles of ceria [63].

Although there was no significant difference in the Zn concentration found in the liver of the mice given doses of either microparticles or nanoparticles (Table 3), only for the latter was steatosis induced, a fact that stresses once again that the ZnO-NPs have an enhanced toxicity compared to the microparticles, as other researches have indicated [45, 64]. These results are consistent with recent studies on the effect of ZnO-NPs on the liver [65]. The liver presents one of the greatest problems for the clinical use of nanoparticles. While there are many studies from the 1970s and 1980s on topics of particle–liver interaction, the conclusions established in that time frame may not be fully applicable to current nanoparticle technologies. Since the size of the particles is less than 100 nm, they are on the same scale as many biological molecules. There is, therefore, a great need to better understand the interactions of nanoparticles with the liver from the organ to cell perspective [66].

Although the exact mechanism by which ZnO-NPs can induce adverse effects on cells is not known, it is suggested that nanoparticles can produce reactive oxygen species (ROS) and thus modulate intracellular calcium concentrations, activate transcription factors and induce cytokine production. ROS can cause damage to the cells by peroxidation of lipids, altering proteins, disrupting DNA, interfering with signaling functions and modulating gene transcription [43, 44, 67]. It is to be expected that ZnO-NPs, administered to the mice in the present study and that reached their liver, produced oxidative stress, inflammation and DNA damage, among other possible events, since these are, as indicated by Knaapen et al. in his work [68], some of the processes that allow understanding the complex cellular mechanism after exposure to nanoparticles.

Specifically, clearance by the liver is influenced by the same nanoparticle characteristics. Considering the two modes of clearance, hepatocyte and Kupffer cell uptake, endocytosis and chemical- or enzyme-mediated degradation of the nanoparticles will follow. Uptake by hepatocytes and Kupffer cells can result in chronic accumulation and induce toxicity. The work of Ballou et al. [69] using fluorescence from PEG-coated quantum dots in the intestines of exposed mice suggests excretion from the liver. However, other studies show that there are no appreciable changes in the levels of nanomaterials found in the liver during the development of short-term and long-term studies [70, 71]. In the work of

Niidome et al. [72], the levels of retention of Au-nanoparticles in the liver varied between 30% of the administered dose to 35%. The above suggests that while excretion may occur, it is slow due to live sequestration after RES uptake. This accounts for the results of bioaccumulation of ZnO particles in the liver of the mice used for this test in this work, and even more so for the doses with ZnO-NPs (see Table 3). Specifically, liver macrophages such as Kupffer cells have been identified in some studies as the primary cellular location in the liver for removing nanoparticles [73] and therefore are currently under study to find out more about nanoparticle–liver interaction [62]. The results indicate that administration of ZnO-NPs transiently inhibited Kupffer cell phagosomal motility and later induced hepatocyte injury. In addition, the data show that diminished Kupffer cell organelle motion correlated with ZnO-NPs-induced liver injury [62]. This effect would be important to justify the results obtained in our work.

Conclusions

The synthesis method used made it possible to obtain spheroidal, uniform nanoparticles of ZnO, with a size of ~ 50 nm and low agglomeration. The ZnO-NPs were produced using ethylene glycol as solvent of synthesis, dissolving zinc acetate in a 1 M concentration and surfactant CTAB in a 10 mM concentration. The study indicated that the initial concentration of zinc precursor [$Zn(CH_3COOH)_2$] exerted an important influence on the average size of the particles. Furthermore, the use of surfactant is desirable, principally to encourage dispersion. Toxicity testing was carried out on the synthesized nanoparticles, as described in the work. Biopsies of livers of mice from the group administered with doses of ZnO-NPs showed a condition known as steatosis. This disease is characterized by the accumulation of fat in the liver cells, a pathological effect at the ultrastructural level that can be related to the substantial bioaccumulation of Zn in the liver, a condition that was determined by atomic absorption testing. In the ultrastructural analysis of the kidney, no significant pathological changes were observed, even though the atomic absorption data indicated a substantial bioaccumulation of Zn in this organ. These results lead us to conclude that with small doses of the ZnO-NPs synthesized in this work, 50 mg ZnO/kg body weight (b.v.), it is possible to observe toxic effects, mainly in the liver of the mice that were given this dose. It is therefore necessary to consider, in future nanotoxicity studies, the importance of dose metrics rather than following conventional methods while conducting in vivo experiments.

Acknowledgements This project was funded through project ID 3978. We are grateful to the University of Cauca for making their laboratory facilities available for carrying out this work. We are especially grateful to Colin McLachlan for suggestions relating to the English text.

References

1. Brown, H.E.: Zinc oxide: properties and applications. International Lead Zinc Research Organization, New York (1976)
2. Ozgur, U., et al.: A comprehensive review of ZnO materials and devices. J. Appl. Phys. **98**(4), 041301 (2005)
3. Klingshirn, C.: ZnO: from basics towards applications. Phys. Status Solid B **244**(9), 3027–3037 (2007)
4. Klingshirn, C.: ZnO: material, physics and applications. Chem. Phys. Chem. **8**(6), 782–803 (2007)
5. Moezzi, A., McDonagh, A.M., Cortie, M.B.: Zinc oxide particles: synthesis, properties and applications. Chem. Eng. J. **185–186**, 1–22 (2012)
6. Djurisic, A.B., Leung, Y.H.: Optical properties of ZnO nanostructures. Small **2**, 944–961 (2006)
7. Jagadish, C., Pearton, S.J. (eds.): Zinc oxide bulk, thin films and nanostructures: processing, properties and applications. Elsevier Ltd., Amsterdam (2006)
8. Sun, X.W., Yan, Y.: ZnO nanostructures and their applications. CRC Press Taylor & Francis Group LLC, Boca Raton (2012)
9. Klingshirn, C.F., et al.: Zinc oxide: from fundamental properties towards novel applications. Springer series in materials science, vol. 120. Springer, Heidelberg (2010)
10. Janotti, A., Van der Walle, C.G.: Fundamentals of zinc oxide as a semiconductor. Rep. Prog. Phys. **72**, 126501 (2009)
11. Morkoc, H., Ozgur, U.: Zinc oxide: fundamentals, materials and device technology. Wiley-VCH Verlag & Co. kGaA, Weinheim (2009)
12. Wöll, C.: The chemistry and physics of zinc oxide surfaces. Prog. Surf. Sci. **82**, 55–120 (2007)
13. Lead, J.R., Smith, E.: Environmental and human health impacts of nanotechnology. John Wiley & Sons Ltd Publication, West Sussex (2009)
14. Pichat, P. (ed.): Photocatalysis and water purification, materials for sustainable energy and development. WILEY-VCH Verlag Gmbh & Co. kGaA, Weinheim (2013)
15. Kisch, H.: Semiconductor photocatalysis: principles and applications. WILEY-VCH Verlag Gmbh & Co. kGaA, Weinheim (2015)
16. Vogel, D., Krüger, P., Pollmann, J.: Ab initio electronic—structure calculations for II–VI semiconductors using self-interaction-correction pseudopotentials. Phys. Rev. B **52**, R14316 (1995)
17. Patnaik, P.: Handbook of inorganic chemicals. McGraw Hill, New York (2003)
18. Nohynek, G.J., et al.: Grey goo on the skin? Nanotechnology, cosmetic and sunscreen safety. Crit. Rev. Toxicol. **37**, 251–277 (2007)
19. Choi, S.J., Choy, J.H.: Biokinetics of zinc oxide nanoparticles: toxicokinetics, biological fates, and protein interaction. Int. J. Nanomed. **9**(suppl 2), 261–269 (2014)
20. Liu, J., et al.: The toxicology of ion-shedding zinc oxide nanoparticles. Crit. Rev. Toxicol. **46**(4), 348–384 (2016)
21. Jiang, J.K., Oberdorster, G., Biswas, P.: Characterization of size, surface charge, and agglomeration state of nanoparticle

dispersions for toxicological studies. J. Nanopart. Res. **11**, 77–89 (2009)
22. Yan, H., et al.: Comparative study of cytotoxicity, oxidative stress and genotoxicity induced by four typical nanomaterials: the role of particle size, shape and composites. J. Appl. Toxicol. **29**, 69–78 (2009)
23. Aula, S., et al.: Biological interactions in vitro of zinc oxide nanoparticles of different characteristics. Mater. Res. Express. **1**, 035041 (2014)
24. Shen, C., et al.: Relating cytotoxicity, zinc ions, and reactive oxygen in ZnO nanoparticle-exposed human immune cells. Toxicol. Sci. **136**(1), 120–130 (2013)
25. Eixenberger, J.E., et al.: Rapid dissolution of ZnO nanoparticles induced by biological buffers significantly impacts cytotoxicity. Chem. Res. Toxicol. **30**, 1641–1651 (2017)
26. Kolodziejczak-Radzimska, A., Jesionowski, T.: Zinc oxide—from synthesis to application: a review. Materials **7**, 2833–2881 (2014)
27. Rodríguez-Páez, J.E., et al.: Controlled precipitation methods: formation mechanism of ZnO nanoparticles. J. Eur. Ceram. Soc. **21**, 925–930 (2001)
28. Moharram, A.H., et al.: Direct precipitation and characterization of ZnO nanoparticles. J. Nanomater. (2014). https://doi.org/10.1155/2014/716210
29. Wang, M.H., Ma, X.Y., Zhou, F.: Synthesis and characterization of monodispersed spherical ZnO nanocrystals in an aqueous solution. Mater. Lett. **142**, 64–66 (2015)
30. Avila, H., et al.: Estudio comparativo de dos métodos de síntesis para la obtención de polvos cerámicos de ZnO–Pr_2O_3–CoO. Bol. Soc. Esp. Ceram. **43**(4), 740–744 (2004)
31. Guao, J., Peng, C.: Synthesis of ZnO nanoparticles with a novel combustion method and their C_2H_5OH gas sensing properties. Ceram. Int. **41**, 2180–2186 (2015)
32. Alwan, R.M., et al.: Synthesis of zinc oxide nanoparticles via sol-gel route and their characterization. Nanosci. Nanotechnol. **5**(1), 1–6 (2015)
33. Yang, L., Wang, J., Xiang, L.: Hydrothermal synthesis of ZnO whiskers from ε—Zn(OH)2 in NaOH/Na2SO4 solution. Particuology **19**, 113–117 (2015)
34. Ocakoglu, K., et al.: Microwave-assisted hydrothermal synthesis and characterization of ZnO nanorods. Spectrochim. Acta Part A Mol. Biomol. Spectrosc. **148**, 362–368 (2015)
35. Manzoor, U., et al.: Antibacterial, structural and optical characterization of mechano-chemically prepared ZnO nanoparticles. PLoS One **11**(5), e0154704 (2016)
36. Yu, H., et al.: Synthesis of flower-like ZnO nanostructures by sonochemical route and their photocatalytic activity. Optik **126**, 4397–4400 (2015)
37. Li, Y., Liu, C.S.: Hydro/solvo-thermal synthesis of ZnO crystallite with particular morphology. Trans. Nonferrous Met. Soc. China **19**, 399–403 (2009)
38. Dakhlaoui, A., et al.: Synthesis, characterization and optical properties of ZnO nanoparticles with controlled size and morphology. J. Cryst. Growth **311**, 3989–3996 (2009)
39. Wang, Y.D., et al.: Preparation of nanocrystalline metal oxide powders with the surfactant-mediated method. Inorg. Chem. Commun. **5**, 751–755 (2002)
40. Salem, J.K., Hammad, T.M.: The effect of surfactants on the particle size and optical properties of precipitated ZnO nanoparticles. J. Mater. Sci. Eng. **3**(12), 38–43 (2009)
41. Karakoti, A.S., et al.: Preparation and characterization challenges to understanding environmental and biological impacts of ceria nanoparticles. Surf. Interface Anal. **44**(8), 882–889 (2012)
42. Kumar, A., et al.: Behavior of nanoceria in biologically-relevant environments. Environ. Sci. Nano **1**, 516–532 (2014)
43. Oberdörster, G., Oberdörster, E., Oberdörster, J.: Nanotoxicology: an emerging discipline evolving from studies of ultrafine particles. Environ. Health Perspect. **113**(7), 823–839 (2005)
44. Oberdörster, G.: Safety assessment for nanotechnology and nanomedicine: concepts of nanotoxicology. J. Intern. Med. **267**(1), 89–105 (2010)
45. Wang, B., et al.: Acute toxicity of nano- and micro-scale zinc powder in healthy adult mice. Toxicol. Lett. **161**, 115–123 (2006)
46. Sharma, V., et al.: Induction of oxidative stress, DNA damage and apoptosis in mouse liver after sub-acute oral exposure to zinc oxide nanoparticles. Mutat. Res. **745**, 84–91 (2012)
47. Zhang, J., et al.: Toxic effect of different ZnO particles on mouse alveolar macrophages. J. Hazard. Mater. **219–220**, 148–155 (2012)
48. Pasupuleti, S., et al.: Toxicity of zinc oxide nanoparticles through oral route. Toxicol. Ind. Health **28**(8), 675–686 (2012)
49. Campo, E.J.A., et al.: Room temperature synthesis of high purity 2D ZnO nanoneedles. J. Ceram. Process. Res. **10**(4), 477–481 (2009)
50. OECD-420, OECD guideline for the testing of chemicals: acute oral toxicity fixed dose procedure, 2001, 27OECD. Guidance document on the recognition, assessment and use of clinical signs as humane endpoints for experimental animals used in safety evaluation. Environmental health and safety monograph series on testing and assessment no 19. (2000)
51. OECD-420, OECD guideline for the testing of chemicals: acute oral toxicity fixed dose procedure, 2001, 27OECD. Guidance document on the recognition, assessment and use of clinical signs as humane endpoints for experimental animals used in safety evaluation. Environmental health and safety monograph series on testing and assessment. (2000)
52. Bozzola, J.J., Russell, L.D.: Electron microscopy: principles and techniques for biologists, 2nd edn, pp. 14–37. Jones and Bartlett Publishers Inc., Sudbury (1999)
53. Van Loon, J.C.: Analytical methods for atomic absorption spectroscopy. Academic Press Inc, New York (1980)
54. Greenwood, N.N., Earnshaw, A.: Chemistry of the elements. Butterworth-Heinemann Ltd., Oxford (1984)
55. Pan, Z., et al.: Spontaneous growth of $ZnCO_3$ nanowires on ZnO nanostructures in normal ambient environment: unstable ZnO nanostructures. Chem. Mater. **22**, 149–154 (2010)
56. Maensiria, S., Laokula, P., Promarak, V.: Synthesis and optical properties of nanocrystalline ZnO powders by a simple method using zinc acetate dihydrate and poly(vinyl pyrrolidone). J. Cryst. Growth **289**, 102–106 (2006)
57. Wang, J., et al.: Effect of surfactant on the morphology of ZnO nanopowders and their application for photodegradation of Rhodamine B. Powder Technol. **286**, 269–275 (2015)
58. Israelachvili, J.N.: Intermolecular and surface forces, 3rd edn. Elsevier-Academic Press, Amsterdam (2011)
59. Mathews, C.K., et al.: Biochemistry, 4th edn. Pearson Education, London (2012)
60. Ma, H., et al.: Comparative phototoxicity of nanoparticle and bulk ZnO to a free-living nematode *Caenorhabditis elegans*: the importance of illumination mode and primary particle size. Environ. Pollut. **159**(6), 1473–1480 (2011)
61. Xia, T., et al.: Comparison of the mechanism of toxicity of zinc oxide and cerium oxide nanoparticles based on dissolution and oxidative stress properties. ACS Nano **2**, 2121–2134 (2008)
62. Watson, C.Y., et al.: Effects of zinc oxide nanoparticles on Kupffer cell phagosomal motility, bacterial clearance, and liver function. Int. J. Nanomed. **10**, 4173–4184 (2015)
63. Tseng, M.T., et al.: Persistent hepatic structural alterations following nanoceria vascular infusion in the rat. Toxicol. Patholog. **42**(6), 984–996 (2014)

64. Jiang, W., Mashayekhi, H., Xing, B.: Bacterial toxicity comparison between nano- and micro-scaled oxide particles. Environ. Pollut. **157**, 1619–1625 (2009)
65. Zhang, Y.N., et al.: Nanoparticles—liver interactions: cellular uptake and hepatobiliary elimination. J. Control. Release **240**, 332–348 (2016)
66. Almansour, M.I., et al.: Zinc oxide nanoparticles hepatotoxicity: histological and histochemical study. Environ. Toxicol. Pharmacol. **51**, 124–130 (2017)
67. Xu, X.H., et al.: Real-time probing of membrane transport in living microbial cells using single nanoparticle optics and living cell imaging. Biochemistry **43**, 10400–10413 (2004)
68. Knaapan, A.M., et al.: Inhaled particles and lung cancer. Part A Mech. Int. J. Cancer **109**, 799–809 (2004)
69. Ballou, B., et al.: Noninvasive imaging of quantum dots in mice. Bioconjugate Chem. **15**, 79–86 (2005)
70. Liu, Z., et al.: In vivo bio-distribution and highly efficient tumour targeting of carbon nanotubes in mice. Nat. Nanotechnol. **2**, 47–52 (2007)
71. Fabian, E., et al.: Tissue distribution and toxicity of intravenously administered titanium dioxide nanoparticles in rats. Arch. Toxicol. **82**, 151–157 (2008)
72. Niidome, T., et al.: PEG-modified gold nanorods with a stealth character for in vivo applications. J. Control. Release **114**, 343–347 (2006)
73. Sadauskas, E., et al.: Kupffer cells are central in the removal of nanoparticles from the organism. Part. Fibre Toxicol. **4**, 10 (2007)